DOI: 10.13009/EUCASS2017-265

From high altitude clouds to an icing wind tunnel: en route to understand ice crystal icing

Stephan E. Bansmer⋆† *and Arne Baumert*⋆
⋆*Institute of Fluid Mechanics at Technische Universität Braunschweig*
Hermann-Blenk-Str. 37, 38108 Braunschweig, Germany
s.bansmer@tu-braunschweig.de
†Corresponding author

Abstract

Icing crystal icing is a severe problem for aviation as it can significantly affect the operation of engines and pitot probes. To reproduce such conditions for fundamental research inside an icing wind tunnel environment is challenging. Here, we summarize our efforts of the last five years to upgrade the Braunschweig Icing Wind Tunnel with ice crystal capability and we present both macroscopic and microscopic observations that reveal some of the underlying physical phenomena.

1. Introduction

Icing is a severe problem for aviation as it can significantly affect airworthiness. To better evaluate potential dangers and to support the certification process of new airplanes, the aircraft industry needs predictive tools for ice accretion. Two types of aircraft icing are distinguished: supercooled water droplet icing, which takes place in the lower atmosphere, and ice crystal icing, which is observed in high altitudes of tropical deep convective weather systems. Supercooled means that droplets are in their liquid phase, but have temperatures below the freezing point. Upon impact onto a solid substrate, the drop solidifies due to the heterogeneous nucleation that initiates a fast development of ice dendrites in the liquid.

The process of the ice crystal ice accretion is significantly more complex and is the subject of the present contribution. If the temperature of the solid surface is below freezing, the ice particles ricochet or shatter upon impact, with no significant accretion. However, for surface temperatures above the freezing point, or if a liquid phase is present near/on the ice particle or on the target surface, the impacting ice particle may accrete.[13,14] This is due to the increase of adhesion when thin liquid films are formed in the vicinity of the ice crystals. Warm environments that provoke this behavior can be found in the engine or on heated probes or diagnostic instruments. The growing porous ice layer on engine components leads to a loss of power and efficiency. In severe cases, this leads to engine shutdown. Moreover, a thick ice layer is susceptible for shedding of ice fragments, which then pose a danger for the engine in the form of mechanical damage, increased wear or induced combustion instabilities. Heated measuring probes exposed to such icing conditions can also malfunction, since their surfaces accumulate ice layers.

The following important parameters are of particular significance in defining the boundary conditions of the icing process:

- Classical, fluid-mechanical testing parameters like **Reynolds number** $\mathrm{Re} = \frac{\varrho}{\mu} U_\infty c$, **Mach number** $\mathrm{Ma} = \frac{U_\infty}{a_\infty}$ and **angle of attack** α, where ϱ is the density and μ the dynamic viscosity of air, U_∞ the free-stream velocity, c a reference length of the test article and a_∞ the speed of sound.
- Water concentration in the air. On the one hand, this is the **Liquid Water Content** (LWC), a measure of the mass of water per unit volume of air. Typical values for atmospheric icing conditions range from 0.1 g/m^3 to 3 g/m^3. In the presence of ice crystals, an **Ice Water Content** (IWC) has to be specified. Inside continental and oceanic mesoscale convective systems, IWC-values are range between 0.001 and 1 g/m^3, peek values of 6 g/m^3 have been observed in high tropical convection.[7] Commonly, a **Total Water Content** (TWC) is defined as the sum of water vapor, LWC and IWC.

DOI: 10.13009/EUCASS2017-265

- **Median volume diameter** (MVD) of the statistical distribution of water droplets in the liquid cloud. MVD attempts to reduce the size distribution to a single, representative scalar diameter. In the presence of ice crystals, a **median mass diameter** (MMD) is defined because of their variable density.
- **Static air temperature**. For water droplet icing, static temperatures close to 0°C promote glaze ice formations, at lower static temperatures, rime ice formation becomes predominant.
- **Humidity**, i.e. the amount of water vapor in the air, is an important parameter for mixed-phase ice accretion.[5] Jung et al. showed its relevance for pure droplet icing.[8] A distinction is made between absolute humidity AH and relative humidity RH. Absolute humidity is defined by the mass of water vapor per unit volume of air. With the partial pressure of water vapor p_{vapor}, the static temperature T of air and the specific gas constant of the vapor R_{vapor}, this yields AH $= \frac{p_{\text{vapor}}}{R_{\text{vapor}} T}$. Relative humidity is defined as the ratio of the partial pressure of water vapor p_{vapor} to the equilibrium vapor pressure of water p^*_{vapor}, i.e. RH $= \frac{p_{\text{vapor}}}{p^*_{\text{vapor}}}$.
- **Accumulation time** t_{acc}, for which the model is exposed to the cloud of super-cooled droplets and/or ice crystals.

Experimental studies[4,5,16] indicate that the ratio of the liquid water content (LWC) to the total water content (TWC) has a great influence on ice accretion severity. Currie et al. (2013) proposed a dependency of the relative icing severity on LWC/TWC. Ice accretion is found in the approximate LWC/TWC range 10% to 25%. At low values of LWC/TWC, insufficient liquid is present to result in the ice particles adhering to the surface, whereas when too much liquid is present, the surface is not become sufficiently cooled to result in ice adhesion. Therefore, the lower limit for LWC/TWC arises from the particle impact dynamics, while its upper limit is governed by the heat fluxes affecting the accretion and the substrate underneath it. Clearly the problem is a conjugate heat transfer problem.

In this contribution, selected findings of the icing research in Braunschweig with respect to mixed-phase icing is presented. This comprises a short summary of the efforts to obtain ice crystal icing conditions in the Braunschweig Icing Wind Tunnel, followed by both macroscopic and microscopic observations of the icing process itself. A conclusion will address the direction of future research on that topic.

2. From high altitude clouds to an icing wind tunnel

In the atmosphere, a great variety of ice crystals can be found. Ice crystals grow by incorporation of ambient water vapor. Their primary structure can feature plate, column or hybrid structures and depends on environmental temperature. Secondary crystal structures can be of high complexity for example in case of dendrite crystals. The character of secondary structures is based on the quantity of ambient vapor supersaturation. Temperature and vapor influences on the ice crystal structure can be summarized by the ice crystal morphology diagram shown in figure 1. Plate or columned type crystals correspond to limited temperature ranges. Structural ice particle complexity increases with supersaturation. Hybrid crystals may form if an individual crystal crosses regions of different characteristic temperatures during its growth process.

In order to better document ice crystal icing conditions in deep convective systems, two flight campaigns have been conducted in the course of the HAIC- and HIWC project.[6,15] The first campaign took place in Darwin, Australia in 2014 during the monsoon period, the second campaign in Cayenne, French Guiana, in 2015 during the rainy season. Details about the campaigns and about data treatment can be found in.[10]

Figure 2 shows examples of ice particle images captured close to $-10°\ C$ during the Darwin campaign with the 2D-Stereo probe. Images were recorded in convective cores with IWC peak values exceeding 3 g/m^3. Close to $-10°\ C$, column and capped column type crystals have been found. Larger ice crystals ($> 600\ \mu m$) are rare and resemble graupel (dense and roundish particles).

To reproduce ice crystal icing conditions inside an icing wind tunnel environment, the Braunschweig Icing Wind Tunnel has been upgraded. A comprehensive description of the design, construction and commissioning of the facility is currently in preparation.[1] The overall facility is illustrated in figure 3, the wind tunnel is colored in blue. It is a closed loop wind tunnel, air speeds up to 40 m/s can be adjusted inside the test section that features a cross sectional area of 500 x 500 mm. The wind tunnel can be operated in a static temperature range of $-20°\ C$ to $+30°\ C$. Temperature adjustment is possible by means of an external refrigeration system which is shown in the right side of figure 3. The refrigeration system provides cooling power up to 80 kW. Using a spray bar system, water is atomized at the entry of the wind tunnel nozzle to generate a cloud of supercooled droplets.

DOI: 10.13009/EUCASS2017-265

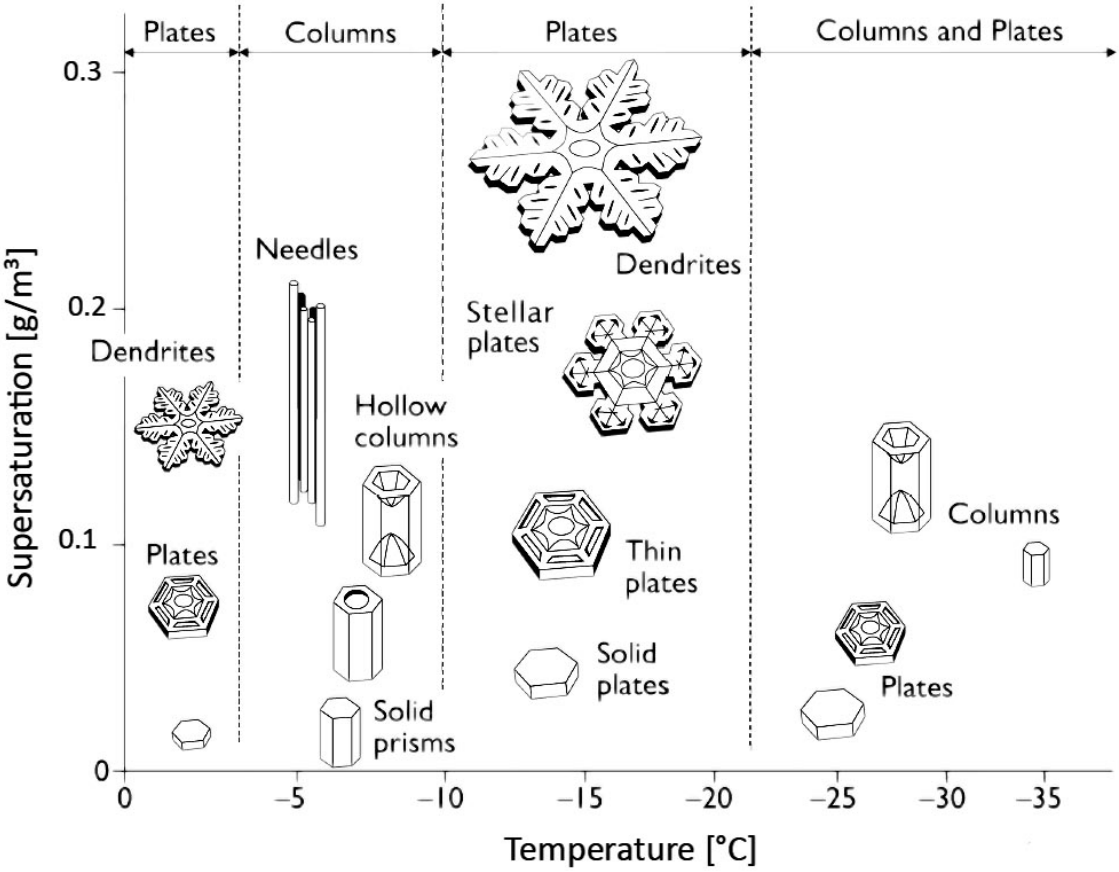

Figure 1: Ice crystal morphology diagram, adapted from Libbrecht.[11]

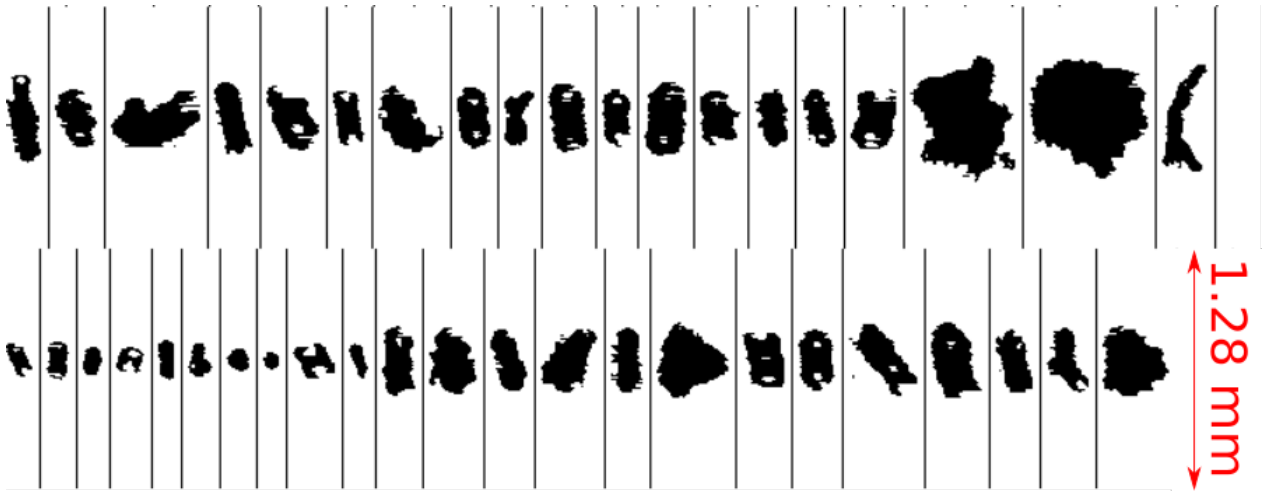

Figure 2: Ice particle images captured by 2DS probe in convective cloud region during Darwin Campaign, $MMD \approx 80\mu m$, $IWC \approx 3.0 g/m^3$, $T_\infty \approx -10°\ C$

DOI: 10.13009/EUCASS2017-265

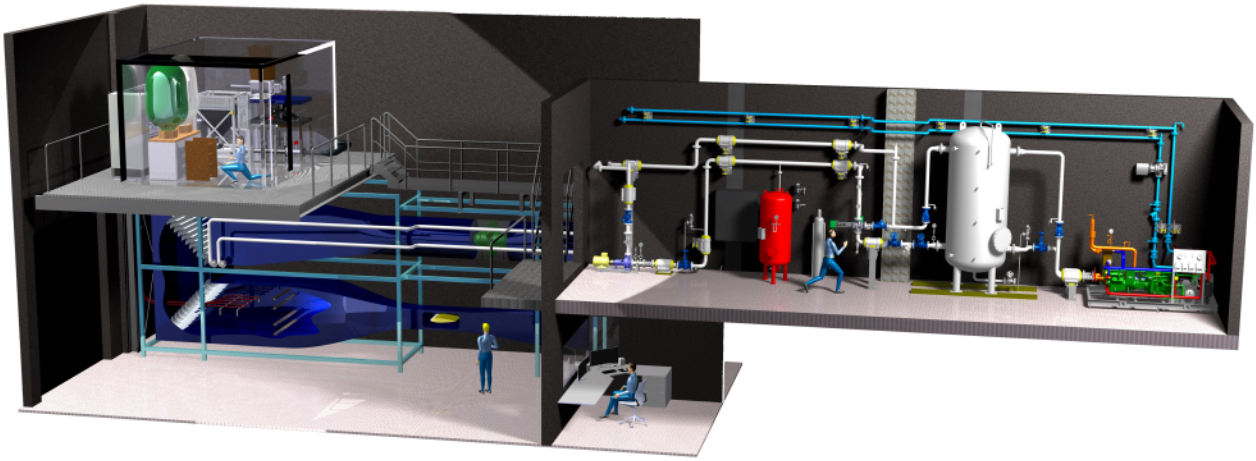

Figure 3: TU Braunschweig Icing Wind Tunnel facility

Replicas of natural ice crystals are produced inside two cloud chambers. Atomized droplets are provided to the cloud chambers by decent conveying air flows. The droplets are forced to freeze out by synchronized expansion of cooled pressurized air inside the chamber. On the expense of ambient vapor and liquid droplets the frozen droplets further grow to naturally shaped ice particles. This procedure exactly matches the growth process of ice crystals in atmospheric clouds. The supply of conveying air and pressurized air to the chamber causes frequent air circulation and keeps the particles moving inside the cloud. As the particles have grown to a critical size, they settle down to the bottom of the chamber. The chamber is directly connected to a chest freezer where the particles are automatically stored. The chest freezers operate at temperatures in the range of -60°C to -70°C. The cold temperature suppresses sintering of the particles to strongly connected aggregates. Nevertheless, the ice crystals degenerate to a certain degree during the storage process.

When sufficient ice particles are stored inside the chest freezers, they can be pneumatically conveyed into the icing wind tunnel. For this purpose, airflow is extracted from the icing wind tunnel by a bypass construction using a radial fan. An aftercooler compensates heat input of the fan and environment. The ice particles are then fed into this cold conveying air stream, which is guided by pipes into the icing wind tunnel. The particles are blown out slightly upstream the spray bar system. Particle dosing is realized by a combination of a volumetric dosing machine and a sieving machine.

The ice particle generation and conveyance system allows to adjust ice water contents in the range of 3 to 20 g/m^3 inside the test section. The ice particle cloud is characterized by a medium mass diameter (MMD) of 80 μm. The particles feature aggregates of tiny ice crystals that have accumulated during storage prior to an experiment. Irregular particle shapes are characteristic and can be maintained during conveyance to the IWT. Figure 4 shows a selection of ice particles images obtained by a 2DS optical array probe[9] inside the test section of the wind tunnel.[1] More detailed information about ice particle generation and mixed phase capabilities are given by Baumert et al.[2,3]

3. Macroscopic Observations

3.1 Experimental Setup

After calibrating the ice crystal cloud, it turned out that the spatial distribution of the IWC is reasonably constant on an area of about $15 \times 15\,\mathrm{cm}^2$ in the middle of the test section and then continuously decays towards the tunnel walls. To minimize three-dimensional heat fluxes in and around the test article due to variations of IWC, its dimensions have to be kept smaller than 15 cm.

Due to available data in the literature, a thin-walled hollow cylinder had been chosen as a test article, see figure 5.

DOI: 10.13009/EUCASS2017-265

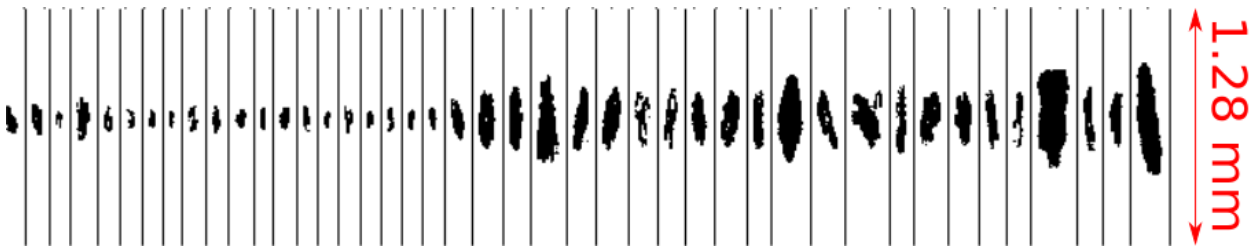

Figure 4: Ice particle images captured by 2D-S probe inside the Braunschweig Icing Wind Tunnel test section, $MMD = 79\mu m$, $IWC = 3.2g/m^3$, $T_\infty = -15°\ C$

Its walls are composed of different layers. The outermost aluminum shell provides a uniform surface quality with good thermal conductivity. To measure the radial temperature gradient, the main aluminum shell is equipped with PT1000 temperature sensors. Outer shell and main shell are glued with Loctite®9497. Heat foils that are insulated towards the inner cylinder wall, provide a reasonable constant heat flux.

With white light, the region of the leading edge is illuminated. A camera observes the ice accretion from the side perspective when the cylinder is exposed to an icing cloud with known LWC, IWC, airspeed U_∞, and static temperature T_∞. The spherical caps on both ends of the cylinder provide a smooth decay of the ice accretion that ensures good optical access to the tunnel center-line.

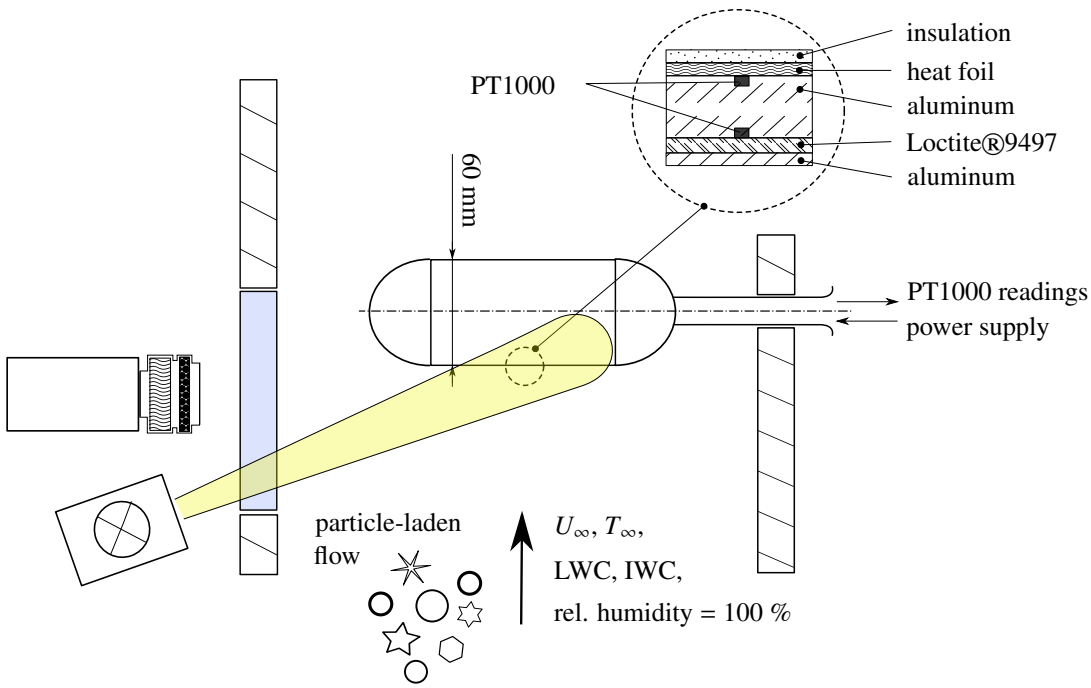

Figure 5: Experimental setup for macroscopic observations of mixed-phase ice accretion.

3.2 Results

Comprehensive investigations on ice accretions of generic test articles at mixed phase conditions have been performed. Figure 6 shows ice accretion shapes on the cylinder model without additional heating. A mixed phase cloud with a total water content of $12g/m^3$ and a melting ratio m_r (defined as LWC/TWC in our setup) of 0.12 had been adjusted. The static temperature had been varied between 0 and -15° C.

In contrast to supercooled droplet icing, the ice accretion for mixed-phase icing exhibit a conical shape. The ice accretion process appears to be strongly dependent on air temperature. At constant melting ratio and constant total

DOI: 10.13009/EUCASS2017-265

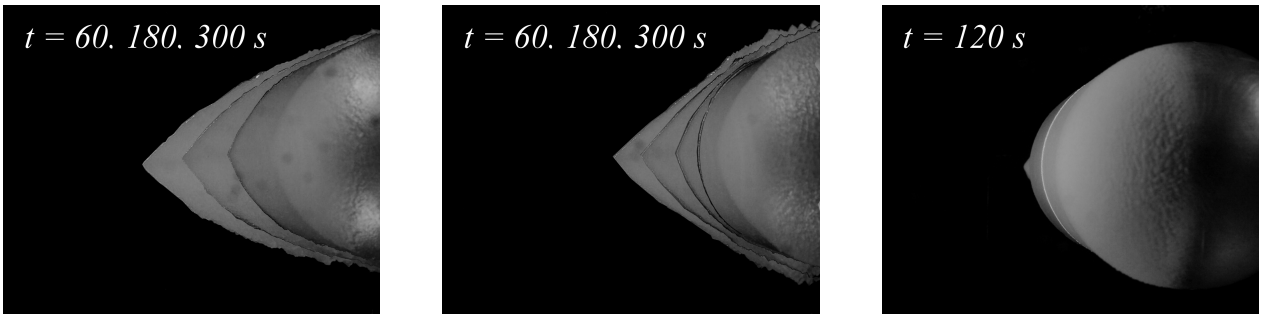

a) $T_\infty = 0\ °C$ b) $T_\infty = -5\ °C$ c) $T_\infty = -15\ °C$

Figure 6: Side view ice accretion shapes at $TWC = 12g/m^3$, $m_r = 0.12$ and $U_\infty = 40\ m/s$, variation of temperature

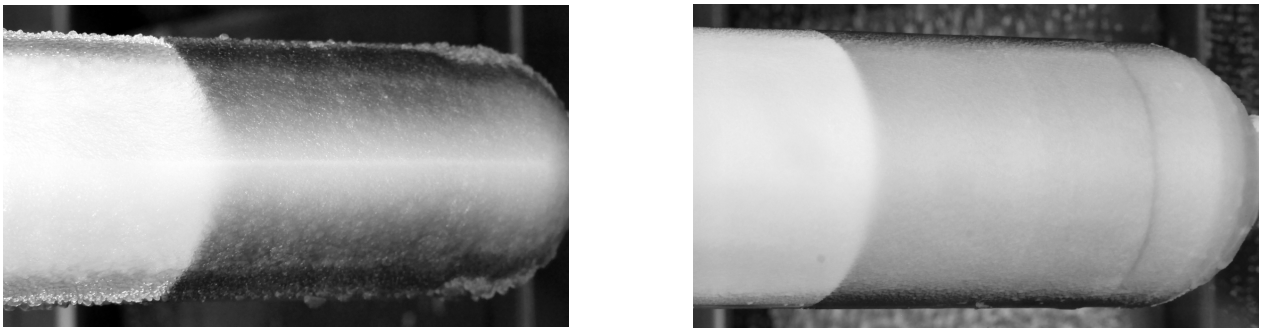

a) $T_\infty = -5°\ C$ b) $T_\infty = -15°\ C$

Figure 7: Front view ice accretion shapes at $TWC = 12g/m^3$ and $m_r = 0.12$, variation of temperature

water content, a decrease in icing severity could be observed for lower temperatures. This effect can be addressed to supercooling of the liquid droplets inside the mixed phase clouds. At lower temperatures enhanced supercooling allows a bigger amount of liquid to freeze with only a short delay upon impact. Therefore, less liquid is locally available to promote ice particle sticking resulting in a significantly reduced ice accretion. Water imbibition into the supposed porous ice layer seems therefore a necessary condition for increased icing severity.

Figure 7 shows cylinder ice accretions from a front view perspective. At $T_\infty = -15°C$ the cylinder is covered uniformly with ice particles incorporated in a thin accretion layer, where effects of liquid supercooling predominate. In contrast, at $T_\infty = -5°C$ the accretion features a very sharp leading edge. Again, this cone type accretion geometry is characteristic for icing at mixed phase conditions which is governed by ice particle impact and sticking.

Figure 8 shows measurements of the temperature near the cylinder surface at the stagnation point as a function of time for two different cases. The left plot corresponds to the non-heated cylinder, with its initial temperature below the freezing point. At $t = 30$s, the cylinder is exposed to the icing cloud. The impact of ice crystals yields a fast decrease in temperature. Since the melting ratio LWC/TWC is zero for this experiment, no ice accretion is observed. When heating the cylinder to an initial temperature of 40 $°C$, see the right plot of figure 8, impacting ice particles are melted due to the heat flux which is caused by the surface temperature above the freezing point. This heat flux is decreasing the surface temperature of the cylinder. When it decreases to a value of about 0 $°C$, ice starts to built up on the target surface close to the stagnation line. This initial layer of ice promotes further sticking of impacting ice crystals.

DOI: 10.13009/EUCASS2017-265

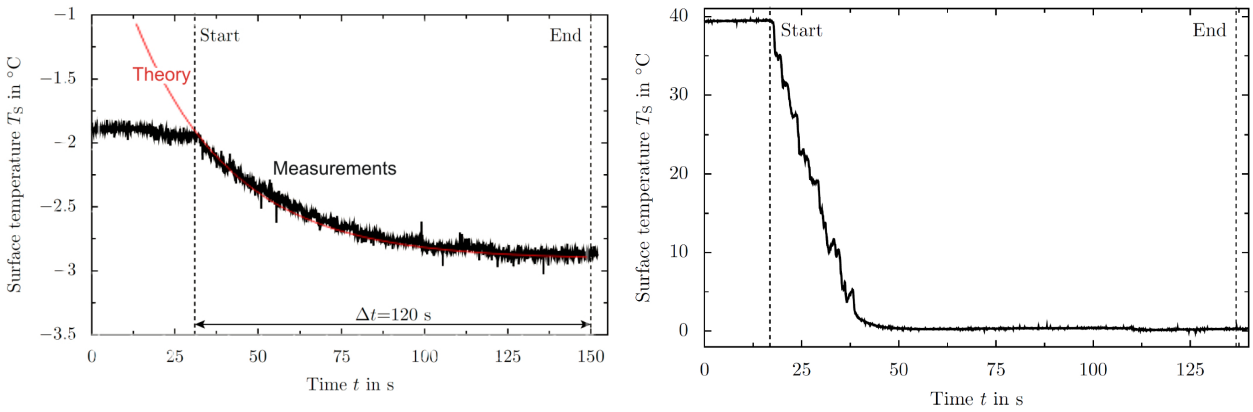

Figure 8: Surface temperature at the stagnation point of the cylinder as a function of time for the non-heated cylinder exposed to an ice crystal cloud, LWC/TWC = 0, in comparison with theoretical predictions (left graph); and heated cylinder impacted at mixed phase conditions, (right graph). Data from Löwe et al.[12]

4. Microscopic Observations

4.1 Experimental Setup

The goal of the microscopic observation is to visualize the temporal evolution of single ice-crystal impacts with a high speed camera. Therefore, the camera lens has to provide sufficient magnification to resolve the ice particles with diameters of about 100 μm. Such lenses usually have a very limited depth of field, which is why the adjacent area to the measurement volume has to be kept clear of any ice accretion. Accordingly, a hemisphere has been used as a test article, see figure 9.

The hemisphere is made out of aluminum, has a diameter of 60 mm and is extended in downstream direction by a cylindrical segment to minimize flow unsteadiness in the vicinity of the stagnation point due to vortex shedding in the wake. The shaddowgraphy setup consists of a SMETEC LED-P40 light source and a Photron FastCAM SA-Z 2100K Monochrom high speed camera.

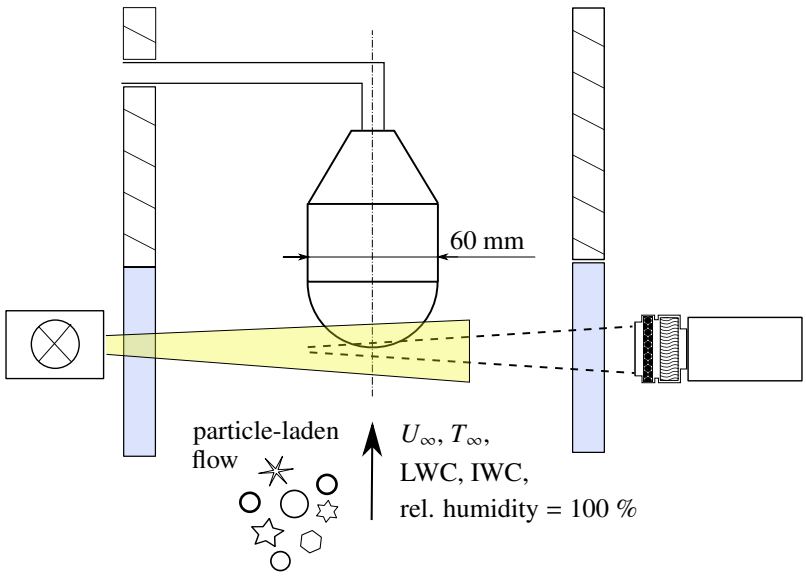

Figure 9: Experimental setup for microscopic observations of glaciated and mixed-phase ice accretion.

DOI: 10.13009/EUCASS2017-265

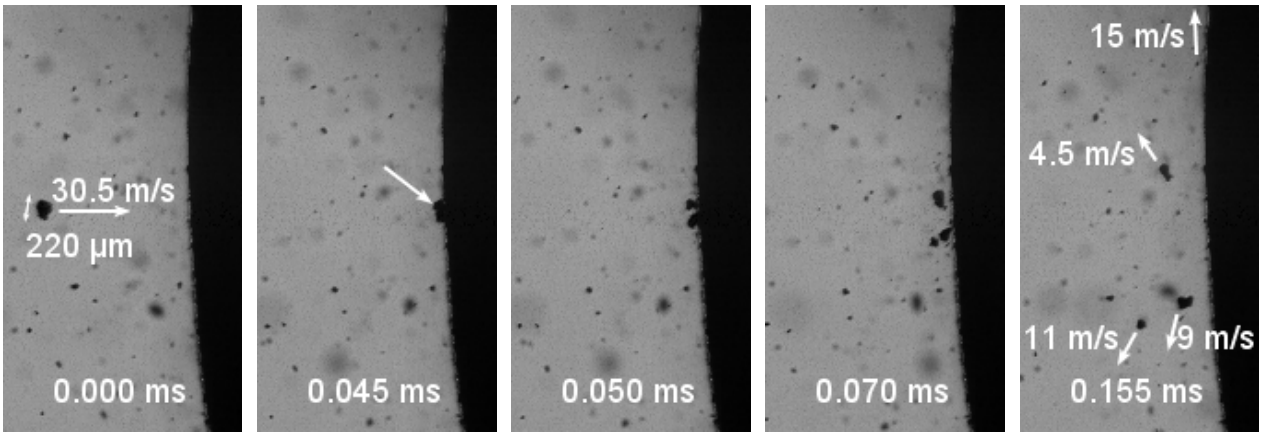

Figure 10: Ice particle impact, $T_\infty = -5°\ C$, $IWC = 9.6\ g/m^3$, glaciated conditions, hemisphere.

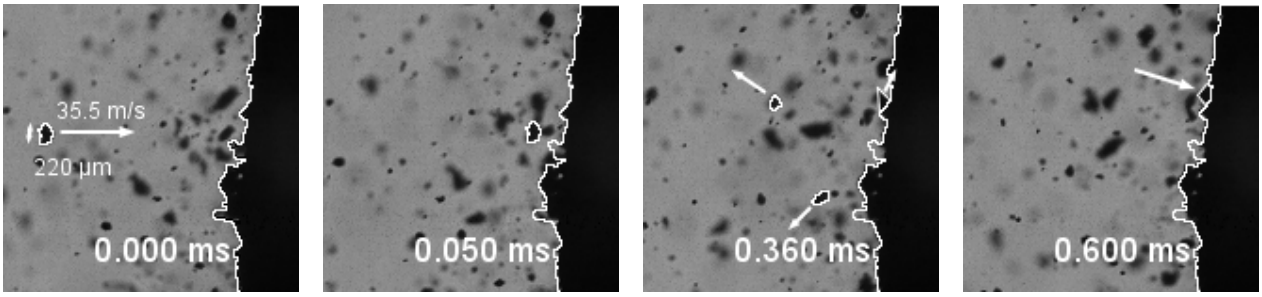

Figure 11: Ice particle impact during mixed phase ice accretion, $T_\infty = -5°\ C$, $TWC = 12\ g/m^3$, $m_r = 0.2$, particle fragmentation with sticking.

4.2 Results

Figure 10 shows a typical impact scenario for glaciated conditions, with $IWC = 9.6\ g/m^3$, $LWC = 0\ g/m^3$, $U_\infty = 40\frac{m}{s}$. The compact ice particle of about 90 μm in size approaches the hemisphere surface with an impact velocity of about 35 m/s. The particle impinges almost normal to the hemisphere surface since the event is located very close to the stagnation point. Even with its compact habit the particle breaks into three main fragments and several minor particles so that the impact can be considered as a catastrophic breakup. The major fragments rebound with angles below 45 ° while the minor fragments move rather parallel to the hemisphere surface. Compared to the major fragments, which rebound with velocities of 4 to 11 m/s, the minor fragments are accelerated to much higher velocities up to 40 m/s. Since the hemisphere is not heated and the static temperature of the air is well below 0 °C, no ice accretion is observed.

Figure 11 shows an example of an impact event at mixed phase conditions during accretion growth. The approaching ice particle of 220 μm in size is highlighted by a white contour and has an impact velocity of about 35.5 m/s. The initial accretion surface at $t = 0$ ms is also highlighted by a white contour in all of the four pictures and features a rather irregular structure with large roughness elements. After impact, the primary particle breaks in three major fragments. Two fragments rebound off the surface into the outer flow field. The 3rd fragment seems to roll over the surface and finally sticks to it due to a spike upside of the impact location.

Having observed many of these impact events, sticking seems to be a statistical event, which is besides the initial particle size and speed depending on the local accretion composition and structure (blocking of horizontally rebounding particles, damping of the actual impact) as well as the shape of the individual particle (impact behavior depending on fragility).

DOI: 10.13009/EUCASS2017-265

5. Conclusion

After being upgraded with ice crystal capability, both macroscopic and microscopic visualization experiments of ice crystal icing have been conducted in the Braunschweig icing wind tunnel. Depending on the boundary conditions, the shape of ice accretion varies between those of classical supercooled icing and ice cones. High-speed visualization of single ice crystal impacts showed a complex behavior of particle interaction with the rough ice surface. This suggests that porous properties of ice including the effects of mechanical damping and water imbibition have to be considered in more detail.

In the future, we want to investigate the ice crystal icing process for a broader range of boundary conditions and create a link to computational modeling efforts aiming to reveal the interplay between the involved phenomena.

6. Acknowledgments

This project has received funding from the European Union's Seventh Framework Programm in research, technological development and demonstration under grant agreement n°ACP2-GA-2012-314314. In this regard, the authors express their thanks to all the project partners from Europe and overseas.

Many thanks to Bastian Hoffmann and Andreas Mangold from VKT Kommunikations GmbH who provided the equipment for the high speed visualization. Further thanks to Jens Löwe (TU Darmstadt) for sharing material of his master thesis.

References

[1] S.E. Bansmer, A. Baumert, S. Sattler, I. Knop, D. Leroy, A. Schwarzenboeck, T. Jurkat, C. Voigt, H. Pervier, and B. Espositio. Design, construction and commissioning of the braunschweig icing wind tunnel. *Journal of Atmospheric and Oceanic Technology*, in preparation for publishing in 2017.

[2] A. Baumert, S. Bansmer, and M. Bacher. Implementation of an innovative ice crystal generation and conveyance system to the icing wind tunnel braunschweig. *53rd AIAA Aerospace Sciences Meeting and Exhibit, AIAA-2015-1225*, January 2015.

[3] A. Baumert, S. Bansmer, S. Sattler, H. Pervier, and B. Esposito. Simulating natural ice crystal cloud conditions for icing wind tunnel experiments - a review on the design, commissioning and calibration of the tu braunschweig ice crystal generation system. *8th AIAA Atmospheric and Space Environmehts Conference, AIAA 2016-4053*, 2016.

[4] T. Currie and D. Fuleki. Experimental results for ice crystal icing on hemispherical and double wedge geometries at varying mach numbers and wet bulb temperatures. *8th AIAA Atmospheric and Space Environmehts Conference, AIAA 2016-3740*, 2016.

[5] T.C. Currie, P.M. Struk, D. Tsao, J-C. Fuleki, and D.C. Knezevici. Fundamental study of mixed-phase icing with application to ice crystal accretion in aircraft jet engines. *4th AIAA Atmoshperic and Space Environments Conference, AIAA-2012-3035*, 2012.

[6] F. Dezitter, A. Grandin, J.L. Brenguier, F. Hervy, H. Schlager, P. Villedieu, and G. Zalamansky. Haic (high altitude ice crystals). *5th AIAA Atmospheric and Space Environments Conference, AIAA-2013-2674*, June 2013.

[7] J-F Gayet, Valery Shcherbakov, Luca Bugliaro, Alain Protat, Julien Delanoë, Jacques Pelon, and Anne Garnier. Microphysical properties and high ice water content in continental and oceanic mesoscale convective systems and potential implications for commercial aircraft at flight altitude. *Atmospheric Chemistry and Physics*, 14(2):899–912, 2014.

[8] Stefan Jung, Manish K Tiwari, N Vuong Doan, and Dimos Poulikakos. Mechanism of supercooled droplet freezing on surfaces. *Nature communications*, 3:615, 2012.

[9] R Paul Lawson, Darren OConnor, Patrick Zmarzly, Kim Weaver, Brad Baker, Qixu Mo, and Haflidi Jonsson. The 2d-s (stereo) probe: Design and preliminary tests of a new airborne, high-speed, high-resolution particle imaging probe. *Journal of Atmospheric and Oceanic Technology*, 23(11):1462–1477, 2006.

DOI: 10.13009/EUCASS2017-265

[10] D. Leroy, E. Fontaine, A. Schwarzenboeck, J.W. Strapp, L. Lilie, J. Delanoe, A. Protat, F. Dezitter, and A. Grandin. Haic/hiwc field campaign - specific findings on psd microphysics in high iwc regions from in situ measurements: Median mass diameters, particle size distribution characteristics and ice crystal shapes, sae technical paper 2015-01-2087. *SAE 2015 International Conference on Icing of Aircraft, Engines and Structures*, June 2015.

[11] K.G. Libbrecht. The physics of snow crystals. *Reports of Progress in Physics*, 68:855–895, March 2005.

[12] Jens Löwe, Daniel Kintea, Arne Baumert, Stephan Bansmer, Ilia V Roisman, and Cameron Tropea. Inception of ice accretion by ice crystal impact. In *Journal of Physics: Conference Series*, volume 745, page 032013. IOP Publishing, 2016.

[13] J.G. Mason, P. Chow, and D.M. Fuleki. Understanding ice crystal accretion and shedding phenomenon in jet engines using a rig test. *Journal of Engineering for Gas Turbines and Power*, 133:041201–1 – 8, 2011.

[14] J.G. Mason, J.W. Strapp, and P. Chow. The ice particle threat to engines in flight. *44th AIAA Aerospace Sciences Meeting and Exhibit, AIAA-2006-206*, June 2006.

[15] JW Strapp, A Korolev, T Ratvasky, R Potts, A Protat, P May, A Ackerman, A Fridlind, P Minnis, J Haggerty, et al. The high ice water content (hiwc) study of deep convective clouds: Science and technical plan. Technical report, FAA Report DOT/FAA/TC-14/31, 2015.

[16] P.M. Struk, A.P. Broeren, J-C. Tsao, M. Vargas, B.W. William, T. Currie, D. Knezevici, and D. Fuleki. Fundamental ice crystal accretion physics studies. *SAE 2011 Interlational Conference on Aircraft and Engine and Ground Deicing, SAE-2011-38-0018*, June 2011.